Dalton Transactions

Cite this: *Dalton Trans.*, 2011, **40**, 5464

www.rsc.org/dalton

PAPER

Structural variations, electrochemical properties and computational studies on monomeric and dimeric Fe–Cu carbide clusters, forming copper-based staple arrays†

Roberto Della Pergola,*[a] Maurizio Bruschi,[a] Annalisa Sironi,[a] Mario Manassero,*[b] Carlo Manassero,[b] Donatella Strumolo,[c] Serena Fedi[d] and Piero Zanello[d]

Received 14th December 2010, Accepted 8th February 2011
DOI: 10.1039/c0dt01766c

The halide ligands of $[Fe_4C(CO)_{12}(CuCl)_2]^{2-}$ (**1**) and $[Fe_5C(CO)_{14}CuCl]^{2-}$ (**2**) can be displaced by N-, P- or S-donors. Beside substitution, the clusters easily undergo structural rearrangements, with loss/gain of metal atoms, and formation of Fe_4Cu/Fe_4Cu_3 metallic frameworks. Thus, the reaction of **1** with excess dppe yielded $[\{Fe_4C(CO)_{12}Cu\}_2(\mu\text{-dppe})]^{2-}$ (**3**). $[\{Fe_4C(CO)_{12}Cu\}_2(\mu\text{-pyz})]^{2-}$ (**4**) was obtained by reaction of **2** with Ag^+ and pyrazine. $[Fe_4C(CO)_{12}Cu\text{-py}]^-$ (**5**) was formed more directly from $[Fe_4C(CO)_{12}]^{2-}$, $[Cu(NCMe)_4]^+$ and pyridine. $[Fe_4Cu_3C(CO)_{12}(\mu\text{-}S_2CNEt_2)_2]^-$ (**6**) and $[\{Fe_4Cu_3C(CO)_{12}(\mu\text{-pz})_2\}_2]^{2-}$ (**7**) were prepared by substitution of the halides of **1** with diethyldithiocarbamate and pyrazolate, in the presence of Cu(I) ions. All of these products were characterized by X-ray analysis. **3** and **4** and **5** are square based pyramids, with iron in the apical sites, the bridging ligands connect the two copper atoms in **3** and **4**. **6** and **7** are octahedral clusters with an additional copper ion held in place by the two bridging anionic ligands, forming a Cu_3 triangle with Cu–Cu distances ranging 2.63–3.13 Å. In **7**, an additional unbridged cuprophilic interaction (2.75 Å) is formed between two such cluster units. DFT calculations were able to reproduce the structural deformations of **3–5**, and related their differences to the back-donation from the ligand to Cu. Additionally, DFT found that, in solution, the tight ion pair $[NEt_4]_2$ **7** is almost isoenergetic with the monomeric form. Thus, **3**, **4** and **7** are entities of nanometric size, assembled either through conventional metal–ligand bonds or weaker electrostatic interactions. None of them allows electronic communication between the two monomeric units, as shown by electrochemistry and spectroelectrochemical studies. (dppe = $PPh_2CH_2CH_2PPh_2$, pyz = pyrazine $C_4N_2H_4$, py = pyridine C_5H_5N, pz = pyrazolate $C_3N_2H_3^-$).

Aggregation of metal clusters with polytopic ligands may represent a chemical approach to the bottom-up preparation of nanostructures with well defined composition, size and shape. In the field of carbonyl clusters, progresses are limited by their scarce propensity to carbonyl substitution and by the lack of suitable soft ligands.[1] These difficulties can be overcome by using heterodentate phosphines[2] or functionalizing the clusters with electrophilic M-L^+ fragments.[3] Potentially, these studies would lead to the obtainment of coordination polymers or molecular wires that, owing to the well known sink behaviour of metal clusters, can find application for nanoelectronic devices.[4] As an example, Fe–Te–Cu[5] and Ru–Te–Cu[6] clusters have been used for the formation of 1D-polymers with dipyridine or halogen bridge, that were found to be semiconductors with dc conductivities on the order of 10^{-2} $\Omega^{-1}cm^{-1}$.

Similarly, having synthesized two Fe–Cu heterometallic clusters, $[Fe_5C(CO)_{14}(CuCl)]^{2-}$ and $[Fe_4C(CO)_{12}(CuCl)_2]^{2-}$,[7] we exploited the reactivity of the latter for the formation of coordination polymers with bifunctional N-donors, such as pyrazine or

[a]*Dipartimento di Scienze dell' Ambiente e del Territorio – Università di Milano Bicocca- piazza della Scienza 1, 20126, Milano, Italy. E-mail: roberto.dellapergola@unimib.it*
[b]*Dipartimento di Chimica Strutturale e Stereochimica Inorganica – Università di Milano, via G. Venezian 21, 20133, Milano, Italy. E-mail: mmanasse@istm.cnr.it*
[c]*Dipartimento di Chimica Inorganica, Metallorganica ed Analitica "Lamberto Malatesta" – Università di Milano, via G. Venezian 21, 20133, Milano, Italy*
[d]*Dipartimento di Chimica dell'Università di Siena, via De Gasperi 2, 53100, Siena, Italy. E-mail: zanello@unisi.it*

† Electronic supplementary information (ESI) available: Figures S1–S5; tables of selected distances, angles and geometric parameters computed by DFT. Crystallographic data for the structural analysis have been deposited with the Cambridge Crystallographic Data Centre, CCDC reference numbers 804302–804306. Copies of this information may be obtained free of charge from: The Director – CCDC, 12 Union Road, Cambridge, CB2 1EZ, UK. Fax. (int code) + 44(1223)336-033 or Email: deposit@ccdc.cam.ac.uk or www:http://www.ccdc.cam.ac.uk. For ESI and crystallographic data in CIF or other electronic format see DOI: 10.1039/c0dt01766c

4,4′-dipyridine.[8] In order to obtain different supramolecular assemblies, we employed other bifunctional ligands (not necessarily linear) and were able to construct some dimeric structures; however, besides the anticipated ligand substitution, we also observed structural rearrangements of the metal core, caused by loss/gain of copper ions. When copper atoms are incorporated in the cluster, they form $Cu_3(\mu\text{-}S_2CNEt_2)_2$ and $Cu_3(\mu\text{-}pz)_2$ units, reminiscent of the staples found in gold nanoparticles.[9]

In this paper we describe the syntheses, the physico-chemical and theoretical characterization and the crystal structures of the resulting derivatives, showing that large molecular clusters of nanometric dimensions can be assembled not only through conventional ligand–metal bonds, but also with weaker interactions, such as attractive forces between equally charged metal ions (usually referred to as metallophilicity).

Results

The syntheses

In the clusters $[Fe_4C(CO)_{12}(CuCl)_2]^{2-}$ (**1**) and $[Fe_5C(CO)_{14}(CuCl)]^{2-}$ (**2**) copper retains its formal (+1) oxidation state and, in keeping with the lability of this metal ion, the chloro ligands can be easily replaced, either directly or by abstraction with Ag^+ or Tl^+. In order to construct oligomeric derivatives, we explored the reactions of **1** and **2** with potentially bidentate ligands typical of the coordination chemistry of copper (dppe,[10] pyrazine,[11] pyrazolate[12] and diethyldithiocarbamate[13]).

However, the reaction of $(NEt_4)_2$**1** with excess dppe, in the presence of Tl^+, is accompanied by loss of copper, and formation of the cationic complex $[Cu(dppe)_2]^+$; the final product is the salt $[Cu(dppe)_2]_2[\{Fe_4C(CO)_{12}Cu\}_2(\mu\text{-dppe})]$ ($[Cu(dppe)_2]_2$**3**), according to the stoichiometry:

$$2\,[Fe_4C(CO)_{12}(CuCl)_2]^{2-} + 5\ \text{dppe} + 4\ Tl^+ \rightarrow [Cu(dppe)_2]_2[\{Fe_4C(CO)_{12}Cu\}_2(\mu\text{-dppe})] + 4\ TlCl$$

The product was characterized by elemental analysis and X-ray diffraction. Attempts to obtain ^{31}P NMR failed, since the spectra only showed a broad signal at *ca.* 10 ppm, attributable to the P atoms of the tetrahedral counterion.[14] The signal of the P atoms in **3** could not be detected, presumably because of the low symmetry of the copper site and the quadrupolar nature of ^{63}Cu and ^{65}Cu.[15]

The reaction of $(NEt_4)_2$**2** with pyrazine, in the presence of excess Ag^+, yielded $(NEt_4)_2[\{Fe_4C(CO)_{12}Cu\}_2(\mu\text{-pyz})]$, ($(NEt_4)_2$**4**) based on the same pentatomic cluster. In this case, the partial fragmentation of the cluster was brought about by the excess of silver ions which may also act as an oxidant. Accordingly, the reaction of $[Fe_4C(CO)_{12}(CuNCMe)_2]$ with pyrazine, in the absence of Ag^+, yielded zigzag chains of $[\{Fe_4C(CO)_{12}Cu_2\}(pyz)]_\infty$.[8]

In order to test a more general method for the preparation of $[Fe_4C(CO)_{12}Cu\text{-}L]^-$ clusters and to prepare a monomeric compound, to be used as a reference for electrochemical studies, we reacted $[Fe_4C(CO)_{12}]^{2-}$, $[Cu(NCMe)_4]^+$ and pyridine in THF at room temperature and obtained $[Fe_4C(CO)_{12}Cu\text{-}py]^-$ (**5**). The reaction is straightforward, fast and selective but its apparent simplicity is outweighed by the complexity of the synthesis of $[Fe_4C(CO)_{12}]^{2-}$, which is prepared from $[Fe_6C(CO)_{16}]^{2-}$ by a three step sequence of reactions, including oxidation, protonation and reduction.[16]

We also carried out the substitution of the halides of $(NEt_4)_2$**1** with anionic bifunctional ligands (dithiocarbamate and pyrazolate) in the presence of $[Cu(NCMe)_4]^+$ ions, aiming at the formation of coordination polymers, where neutral clusters, ligands and metal ions could alternate. Instead of the desired chains, we obtained molecular compounds, which were identified by elemental analysis and single crystal X-ray diffraction as $(PPh_4)[Fe_4Cu_3C(CO)_{12}(\mu\text{-}S_2CNEt_2)_2]$ ((PPh_4)**6**), and $(NEt_4)_2[\{Fe_4Cu_3C(CO)_{12}(\mu\text{-}pz)_2\}_2]$ ($(NEt_4)_2$**7**). In these species, the whole bisubstituted cluster $[Fe_4C(CO)_{12}(CuL)_2]^{2-}$ acts as a chelating ligand on a single copper ion, hampering the formation of extended chains. The synthesis of **7** was performed in two steps: in the first, the halides were substituted with neutral pyrazole (pzH); the resulting intermediate neutral cluster $[Fe_4C(CO)_{12}(CupzH)_2]$ was identified from its IR spectrum (ν_{CO} (THF) = 2053(m), 2011(s), 1982(s), 1963(m), 1930(m) cm^{-1}), with no attempt to isolate it. In the second step, $[Cu(NCMe)_4]^+$ was added and the pzH ligands were deprotonated with solid K_2CO_3. In the absence of base, chelation did not occur, since the IR spectra did not show any appreciable variation.

7 was also synthesized from $[Fe_4C(CO)_{12}(CuNCMe)_2]$, pzH, $[Cu(NCMe)_4]^+$ and K_2CO_3. The resulting K_2**7** salt was converted into $[NEt_4]_2$**7** by addition of NEt_4BF_4 in MeOH, to avoid exchange between pz^- and halides. The ^1H NMR of **7** shows three equally intense singlets, in agreement with the solid state structure. The spectrum is invariant upon dilution, and in different solvents (THF and acetone). This result is not very informative, being consistent either with the presence of only one form in those conditions, or with a fast (on the NMR timescale) monomer/dimer equilibrium. To support the spectroelectrochemical findings, anion **7** was reduced with a THF solution of Na-ketyl, while monitoring the solution by IR. The IR spectrum of the reduced product (ν_{CO} bands at 1983, 1963, 1917 cm^{-1}) closely matches that obtained by electrochemical reduction (see later; the shift to higher wave numbers in the chemical reduction is possibly due to the formation of tight ionic couples in the Na^+ salt).[17] The resulting product was oxidized *in situ* with ferrocenium salts, restoring the original spectrum, with only minor traces of decomposition.

The solid state structures

The solid state structures of **3**, **4** and **5** were obtained for the $[Cu(dppe)_2]_2$**3**·2 THF, $[NEt_4]_2$**4** and $[NEt_4]$**5** salts. The first two anions are represented in Fig. 1 and 2, respectively, and **5** is shown in Figure S1 of the Supplementary Material. The cationic complex $[Cu(dppe)_2]^+$ was frequently observed when studying the reactivity of copper and its structure is well known, associated with anionic complexes of copper[10] or other Fe–Cu clusters.[18]

The clusters in **3**, **4** and **5** are constituted by square-based pyramidal metallic frameworks, centred by the interstitial carbide. Fe1 occupies the apical site, and copper is in the basal plane, carrying the bridging ligand. These mixed metal clusters, formally derived from $[Fe_5C(CO)_{14}]^{2-}$,[19] by substitution of one $Fe(CO)_2$ with the isoelectronic CuL fragment, have 74 CVE's as expected.

The main difference in the three structures is in the Fe1–Cu1 bond distance which is shorter in **4** [2.648(1) Å] and longer in **3** and **5** [3.156(1) and 3.178(1) Å respectively], so that the metallic frameworks in the latter two are halfway between square based pyramids and *arachno*-pentagonal bipyramids,[20] with only the

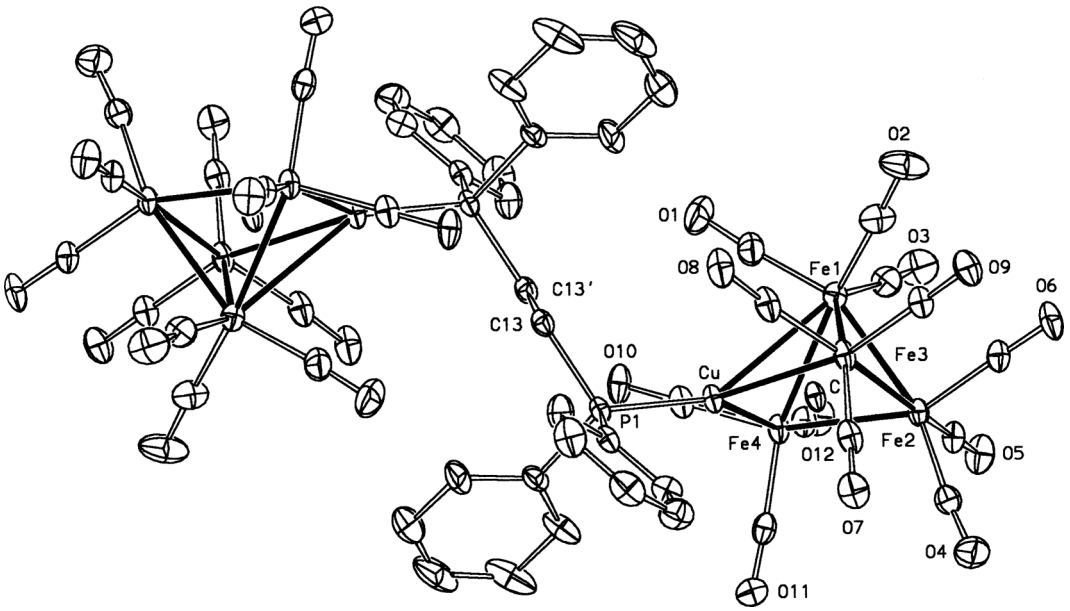

Fig. 1 The solid state structure of $[\{Fe_4C(CO)_{12}Cu\}_2(\mu\text{-dppe})]^{2-}$ (**3**). Ellipsoids are drawn at 30% probability. Primed atoms are generated by the (–x, –y, –1–z) symmetry operation.

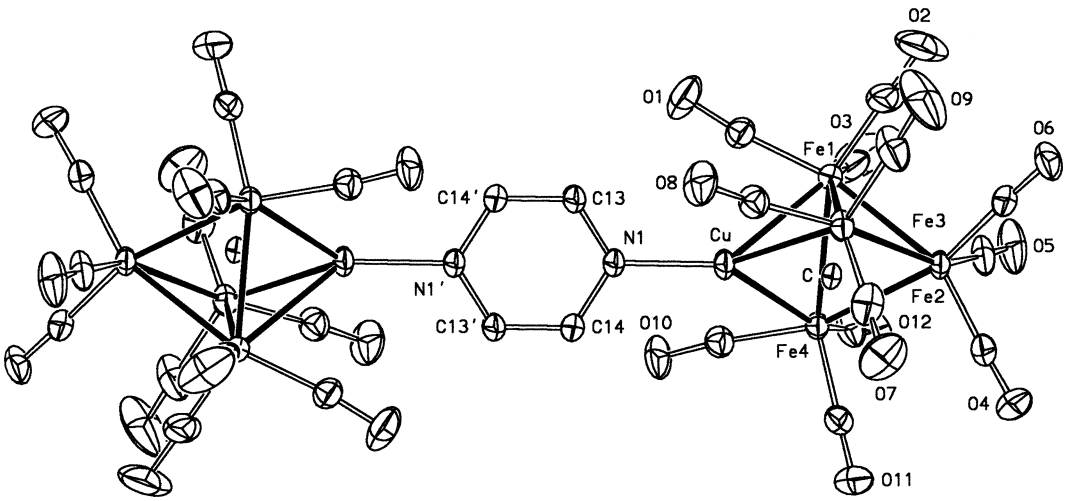

Fig. 2 The solid state structure of $[\{Fe_4C(CO)_{12}Cu\}_2(\mu\text{-pyz})]^{2-}$ (**4**). Ellipsoids are drawn at 30% probability. Primed atoms are generated by the (–x, 1–y, –z) symmetry operation.

two wing tips (Fe3 and Fe4) connected to the bridging copper. However, this pentanuclear geometry should require 76 CVE's.[20,21] Incidentally, the comparison of **4** and **5** (which carry very similar ligands) clearly shows that their structural variations are not due to steric or electronic properties of the ligand, and are more probably the consequence of packing forces. The comparison also allows us to conclude that the Fe–Cu interactions must be very weak and can be easily accommodated, as also observed in the halide substituted **1** and $[\{Fe_4C(CO)_{12}Cu_2(\mu\text{-Cl})\}_2]^{2-}$.[7]

The solid state structures of **6** and **7** were obtained on the $[PPh_4]_2$**6** and $[NEt_4]_2$**7**·CH_2Cl_2 salts. The two species are shown in Fig. 3 and 4, respectively.

The two metallic frameworks are strictly related, both being composed by octahedral Fe_4Cu_2 units, with the Cu–Cu edge spanned by a third copper ion. The latter is held in place by the second atom (either S- or N-) of the two bridging ligands and forced at short distances (2.78–3.14 Å) from the other Cu(I) sites. The Cu3X4 arrays, with their bonding distances, are sketched in Fig. 5. This situation is reminiscent of the "staple" motifs spontaneously formed on gold surfaces [22] and in molecular gold particles[9] (such as $Au_{38}(SR)_{24}$[23] and $[Au_{25}(SR)_{18}]^{-}$[24] (R = CH_2CH_2Ph). These staples not only increase the size of the metallic particles, but are also essential to stabilize the whole molecule, protecting the inner core with multi-ligand structures and widening its HOMO–LUMO gap.[25]

The structures adopted by **6** and **7** confirm that staples with different bridging motifs may be favoured by multidentate ligands, and this idea was indeed recently applied to the synthesis of gold clusters.[26] Moreover, they suggest that these arrays may not be limited to gold, but can be formed also by copper, when the

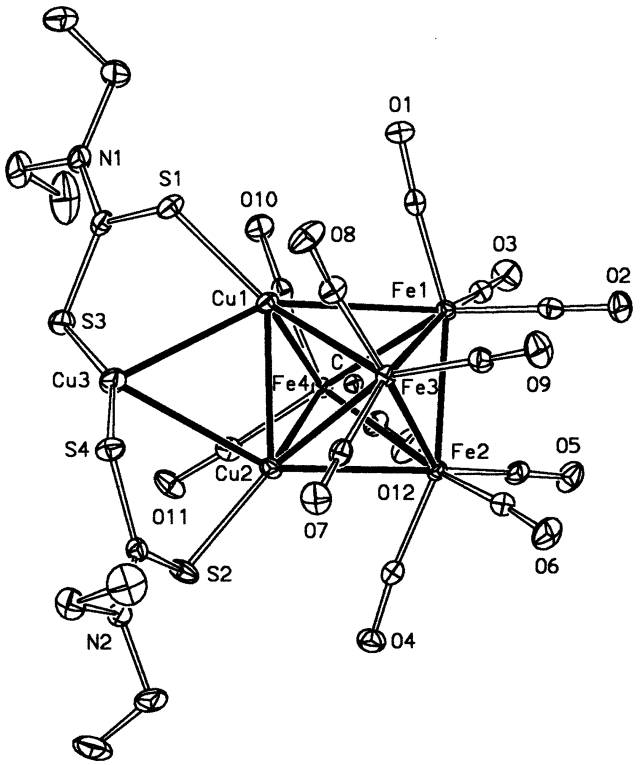

Fig. 3 The solid state structure of $[Fe_4Cu_3C(CO)_{12}(\mu\text{-}S_2CNEt_2)_2]^-$ (**6**). Ellipsoids are drawn at 30% probability.

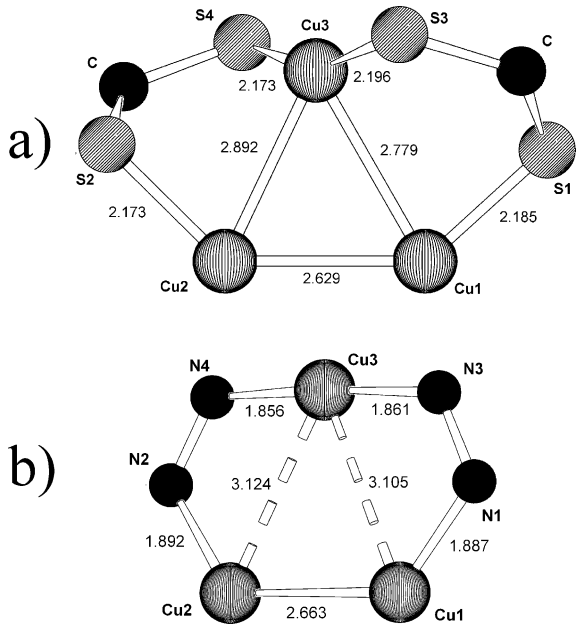

Fig. 5 The staple arrays in **6** (a) and **7** (b) with the relevant bond distances in Å.

contribution of the Cu–Cu bonds to the total energy is expected to be much smaller.[27] The Cu3–Cu6 separation, as determined in the solid state structure of **7**, is relatively short (2.749(1) Å) and, being unsupported by ligands, can be classified as a "cuprophilic" interaction.[27] On that basis, and following the "complex as ligand" approach,[28] **7** can be depicted as a dimeric $(CuL)_2$ unit, where L is the bifunctionalized cluster $[Fe_4C(CO)_{12}(Cu\text{-}pz)_2]^{2-}$, able to chelate two *trans* coordination sites.

The tetrairon units, found in **3–7** are similar to those found in the butterfly $[Fe_4C(CO)_{12}]^{2-}$,[29] and in **1**,[7] including the carbonyl disposition (three for each iron vertex), the short hinges (the Fe1–Fe2 distances are all in the short range 2.52–2.56 Å) and the differences in the Fe–C bonds, which are shorter for the wing tips (1.82–1.83 Å). However, small differences can be appreciated in the Fe1–C distances of the pyramidal (**3–5**) and the octahedral (**6–7**) clusters: in the former Fe1–C are the longest by far (> 1.95 Å, comparable with that found for the apical iron in the homometallic $[Fe_5C(CO)_{14}]^{2-}$[19]). To the contrary, in the octahedra, Fe1–C and Fe2–C are much more similar (about 1.93 Å). Average M–M, M–C, and M–CO distances are compared in Table 1: the values are fairly constant for all the anions even if the Cu–Fe and Cu–Cu bonds show the largest dispersion of data.

Electrochemistry

Fig. 6 illustrates the redox activity of dianion **4** in THF solution. It undergoes a first oxidation possessing features of chemical

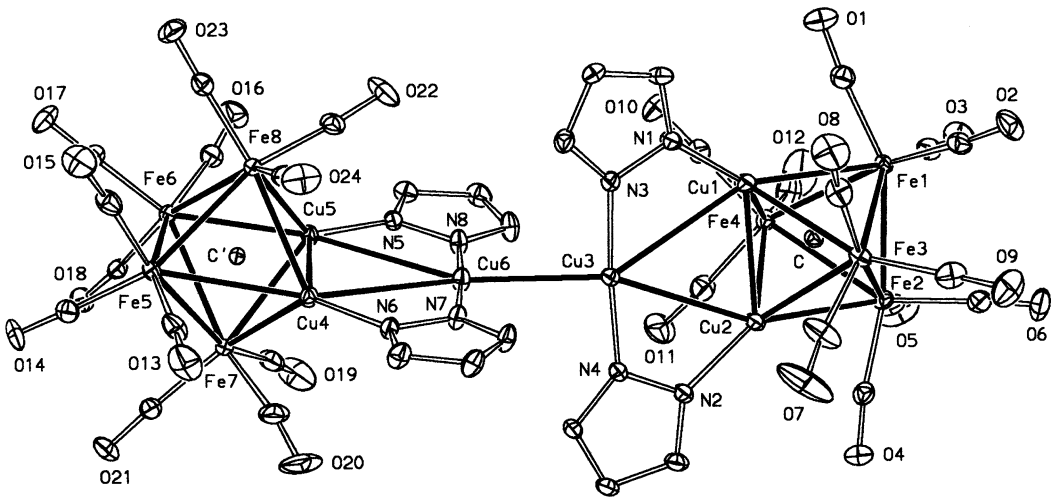

Fig. 4 The solid state structure of $[\{Fe_4Cu_3C(CO)_{12}(\mu\text{-}pz)_2\}_2]^{2-}$ (**7**). Ellipsoids are drawn at 25% probability.

Table 1 Comparison between average bond lengths (in Å) and angles in **3–7**. Figures in parentheses are esd's on unique values, ± numbers are rmsd's on average bond lengths

	3 X = P	**4** X = N	**5** X = N	**6** X = S	**7** X = N
Cu–Cu	—	—	—	2.8 ± 0.1	2.9 ± 0.2
Cu–Fe	2.8 ± 0.3	2.61 ± 0.03	2.8 ± 0.3	2.7 ± 0.1	2.7 ± 0.1
Fe–Fe	2.64 ± 0.06	2.65 ± 0.07	2.64 ± 0.06	2.66 ± 0.06	2.67 ± 0.06
Cu–C	1.901(2)	1.887(3)	1.863(2)	1.909	1.89 ± 0.01
Fe–C	1.88 ± 0.07	1.89 ± 0.08	1.88 ± 0.06	1.90 ± 0.04	1.90 ± 0.03
Cu–X	2.210(1)	1.939(3)	1.926(2)	2.18 ± 0.01	1.88 ± 0.02
Fe–CO	1.78 ± 0.02	1.77 ± 0.02	1.77 ± 0.02	1.79 ± 0.01	1.79 ± 0.01
C–O	1.14	1.15	1.15	1.15	1.15

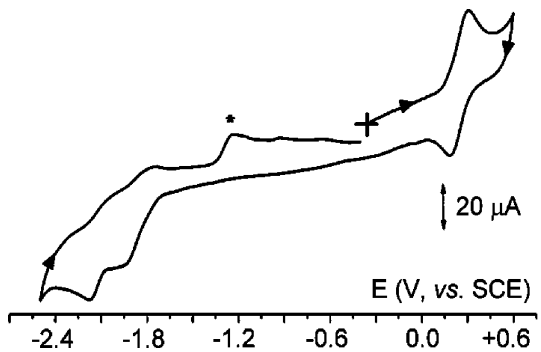

Fig. 6 Cyclic voltammetric response recorded at a gold electrode in THF solution of **4** (0.8×10^{-3} mol dm^{-3}). [NBu_4][PF_6] (0.2×10^{-3} mol dm^{-3}) supporting electrolyte. Scan rate 0.2 V s^{-1}.

Table 2 Formal electrode potentials (V, *vs.* SCE) of the redox changes exhibited by the derivatives under study in different solvents

Complex	E°′ 1st oxidation	E°′ 1st reduction	E°′ 2nd reduction	Solvent
4	+ 0.27	– 1.67	– 1.90	THF
5	+ 0.27	– 1.74	– 1.94	THF
Pyrazine		– 1.57[a]		H_2O
Pyridine		– 2.20[a]		H_2O
1	+ 0.25[b]	– 0.59[b]	– 1.68[b]	CH_3CN
6		– 1.41[c]	– 2.04[c,d]	THF
7	+ 0.70	– 1.23	– 1.58	THF
	+ 0.52	– 1.32	– 1.59	CH_2Cl_2

[a] From Ref. 31; [b] From Ref. 7; [c] Registered at 253 K [d] Peak potential values for irreversible processes (recorded at 0.20 Vs^{-1}).

reversibility in the short times of cyclic voltammetry and two partially reversible reduction processes. Further irreversible anodic processes, not shown in the figure, are also present, and arise from decomposition of the primary oxidation product. In fact, analysis of the voltammetric response of the anodic process with scan rates varying from 0.02 Vs^{-1} to 2.0 Vs^{-1} confirms that the pertinent process is coupled to chemical complications, in that: (i) the current function $i_{pa} \cdot v^{-1/2}$ remains substantially constant; (ii) the current ratio i_{pc}/i_{pa} increases from 0.7 to 0.9; (iii) the peak-to-peak separation increases from 90 mV at 0.02 Vs^{-1} to 150 mV at 2.0 V s^{-1}.[30]

In addition, controlled potential coulometry (E_w = + 0.5 V) consumed more than 6 electrons per molecule, thus suggesting that the instantaneously electrogenerated species tends to decompose affording redox active byproducts. In fact, cyclic voltammetric tests on the resulting solution no longer display the original profile.

Concerned with the two sequential reductions occurring at rather negative potential values, the cyclic voltammetric profile points out that they feature a very limited chemical reversibility. In particular, the most cathodic step gives rise to a kind of stripping peak in the back-scan (asterisked peak), that could arise from reoxidation of adsorbed Cu(0) fragments following the Cu(I)/Cu(0) reduction. From a speculative viewpoint, the presence of an inflection in the voltammetric response of the first reduction (which is more evident in the first derivative deconvolute profile, see Figure S2 in the Supplementary Material†) makes it plausible to assume the involvement of two almost completely overlapping processes.

Although the very negative potentials prevented an accurate determination of the number of electrons involved in such processes by controlled potential coulometry, considering that free pyrazine undergoes reduction at – 1.57 V,[31] and that dinuclear Cu(I) diimines display ligand-based reductions,[32] it does not seem far-fetched to assign the first reduction as ligand centred.

The pertinent electrode potentials are collected in Table 2, together with those of the species that will be discussed below.

Since the IR intervention times are usually short enough to allow the identification of unstable electrogenerated species, the IR spectroelectrochemical investigation corresponding with the oxidation process shows the progressive disappearance of the original ν_{CO} bands at 2039 cm^{-1}, 1989 cm^{-1}, 1966 cm^{-1} and 1910 cm^{-1} in favour of new stretching bands at 2043 cm^{-1}, 2008 cm^{-1}, 1979 cm^{-1} and 1928 cm^{-1}, respectively, which are attributed to the electrogenerated monoanion [{$Fe_4C(CO)_{12}Cu$}$_2$(μ-pyz)]$^-$ (**4**$^-$), Fig. 7.

The concomitant formation of the isosbestic points at 1984 cm^{-1} and 1975 cm^{-1} somewhat supports the relative stability of the monoanion **4**$^-$, even if the pertinent bands are less intense than the original ones. In further confirmation that the primary anodic process is accompanied by a relatively slow molecular reorganization, a new band tends to appear (at 1959 cm^{-1}) whereas all the original bands progressively disappear (Figure S3 in Supporting Material†).

The shift of the CO bands joint to the fact that [$Fe_4C(CO)_{12}$]$^{2-}$ undergoes a series of anodic processes, the first of which likely generates the partially stable monoanion [$Fe_4C(CO)_{12}$]$^-$,[33] makes it plausible to assume that the first oxidation is Fe_4C centred. In this light, the occurrence of a single anodic process supports the conclusion that the two Fe_4C groups in the dimer **4** are not electronically communicating. On the other hand, such a conclusion is also held in the case of related Fe–Cu octahedral carbide clusters.[7]

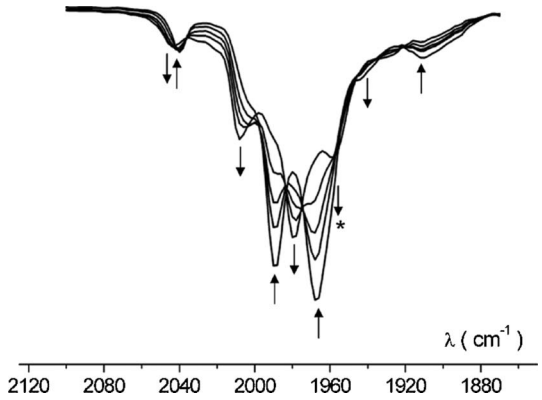

Fig. 7 IR spectroelectrochemical trend in the terminal ν_{CO} region recorded in correspondence of the anodic oxidation of **4** in an OTTLE cell. Step-by-step variation (250 μV s^{-1}) of the potential from E_w = + 0.10 V to E_w = + 0.50 V (V *vs.* pseudo-reference Ag electrode). THF solution containing $[NBu_4][PF_6]$ (0.4 mol dm^{-3}) supporting electrolyte.

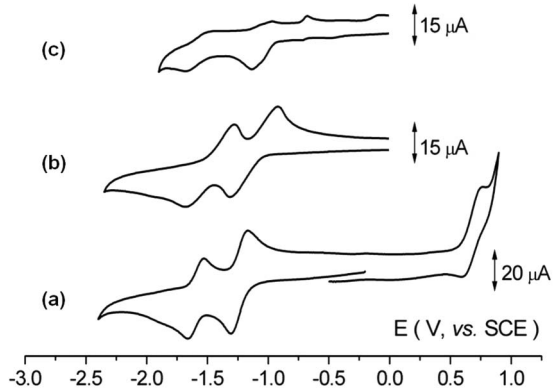

Fig. 8 Cyclic voltammetric responses recorded at a glassy carbon electrode in THF solution of: (a, b) **7** (0.5×10^{-3} mol dm^{-3}); (c) **6** (0.7×10^{-3} mol dm^{-3}). $[NBu_4][PF_6]$ (0.2×10^{-3} mol dm^{-3}). Scan rate 0.2 V s^{-1}. (a) T = 293 K; (b, c) T = 273 K.

The pertinent ν_{CO} bands are collected in Table 3, together with those of the species that will be discussed below. In conclusion, it does not seem too ventured that the LUMO of the dianion **4** is mainly contributed by the Cu–pyrazine–Cu fragment, whereas the HOMO receives the main contribution from the Fe_4C cluster. Let us finally pass to **7**. As illustrated in Fig. 8, which compares its cyclic voltammetric response with that of the monoanion **6** (which can be roughly assumed as the monomer of **7**), the complex exhibits a remarkable electron transfer activity, in that it undergoes one oxidation and two reductions, all the processes possessing features of chemical reversibility.

Unfortunately, any attempt to determine the number of electrons involved in each reduction process failed because of fast re-oxidation of the electrogenerated species, probably due to traces of air. Nevertheless, some evidence can be gained by comparison with the response of **6**. As shown in Fig. 8c, the monoanion undergoes two cathodic processes at about the same potential values as **7**, but they possess a lower extent of chemical reversibility, probably because of the higher stabilization imparted to the dianion by the pyrazolate ligand with respect to the dithiocarbamate ligand.

The partial chemical reversibility and electrochemical quasi-reversibility of the first reduction exhibited by **6** is testified by the analysis of the voltammetric response with scan rates varying from 0.02 Vs^{-1} to 5.0 Vs^{-1}, which shows that: (i) the current function $i_{pa} \cdot v^{-1/2}$ remains substantially constant; (ii) the current ratio i_{pa}/i_{pc} increases from 0.4 to 1.0; (iii) the peak-to-peak separation increases from 150 mV at 0.02 V s^{-1} to 350 mV at 2.0 V s^{-1}. In contrast, the second reduction is completely irreversible. Since controlled potential coulometry (E_W = − 1.70 V) consumes one electron per molecule, the comparison of the peak heights of equimolar amounts of dimer and monomer suggests that the first reduction (as well as the second reduction) of **7** involves two-electrons/molecule. On this basis, it appears that the two carbonyl cluster subunits in **7** are not electronically communicating.

Fig. 9 shows the overall IR spectroelectrochemical profiles recorded for the progressive reduction of both **6** and **7**, corresponding with the first cathodic process.

As in the case of **4**, the one-electron reduction of **6** shows that the original terminal ν_{CO} bands at 2041 cm^{-1}, 1996 cm^{-1}, 1972 cm^{-1} and 1929 cm^{-1} disappear in favour of new stretching bands at 2028 cm^{-1}, 1980 cm^{-1}, 1957 cm^{-1}, and 1907 cm^{-1}, respectively. The concomitant formation of the isosbestic points at 2035, 1987, 1977, 1965 and 1919 cm^{-1} allow us to assign the spectral trend to the electrogeneration of dianion $[Fe_4Cu_3C(CO)_{12}(\mu\text{-}S_2CNEt_2)_2]^{2-}$ ($\mathbf{6}^{2-}$).

It is noted that the shift of about 20 cm^{-1} towards lower wavelengths upon one-electron addition is reminiscent of the behaviour of high-nuclearity platinum carbonyl clusters upon reduction.[34]

Concerning the IR spectroelectrochemical investigation of **7** illustrated in Fig. 9b, the first two-electron process shows that the bands at 2046 cm^{-1}, 2002 cm^{-1} and 1975 cm^{-1} decrease while new bands at 1952 cm^{-1} and 1926 cm^{-1} appear. Also in this case, the appearance of isosbestic points at 1960 cm^{-1}

Table 3 IR stretching frequencies (cm^{-1}) of the terminal carbonyl groups for the cluster under inspection. THF solution containing $[NBu_4][PF_6]$ (0.4 mol dm^{-3}) supporting electrolyte

Cluster	Charge	ν^t_{CO}					
{**4**}	1–[a]	2043	2008	1979	1928		
	2–	2039	1989	1966	1910		
{**6**}	1–	2041	1996	1972	1929		
	2–[a]	2028	1980	1957	1907		
{**7**}	2–	2046	2002	1975	1954	1931	
	4–[a]	2046	2002	1975	1952	1926	
	6–[a]	2046[b]	2002[b]	1975[b]	1952	1926	1880[c]

[a] Electrogenerated in OTTLE cell; [b] Very attenuated; [c] Resulting from overlapping peaks.

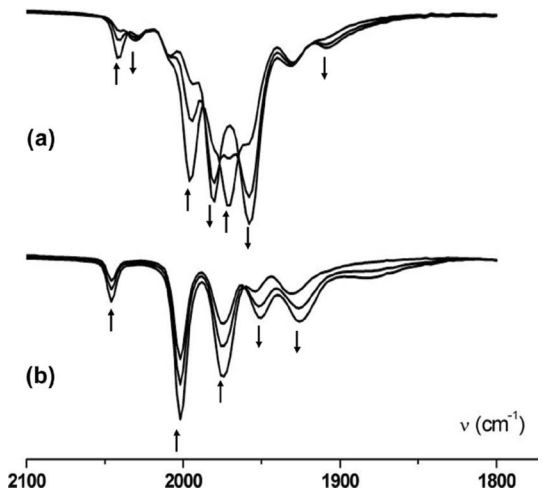

Fig. 9 IR spectroelectrochemical trends in the terminal ν_{CO} region recorded in an OTTLE cell corresponding with the first reduction of: (a) **6**; (b) **7**. Stepwise variation (250 μV s^{-1}) of the potential from E_w = – 1.00 V to E_w = – 1.15 V (a) and from E_w = – 1.00 V to E_w = – 1.30 V (b). V *vs.* pseudo-reference Ag electrode. THF solution containing $[NBu_4][PF_6]$ (0.4 mol dm^{-3}) supporting electrolyte.

supports the relative stability of the electrogenerated species $[\{Fe_4Cu_3C(CO)_{12}(\mu\text{-}pz)_2\}_2]^{4-}$ (**7**$^{4-}$). Upon assuming that the new bands at 1952 cm^{-1} and 1926 cm^{-1} arise from the shift of the two major bands at 2002 cm^{-1} and 1975 cm^{-1} caused by the two-electron addition, it follows that the shifts are of about 50 cm^{-1}, *i.e.* once again about 20 cm^{-1} per electron. In addition the final profile shows that the original bands (2002 cm^{-1} and 1975 cm^{-1}) halve in magnitude in favour of the new bands (1952 cm^{-1} and 1926 cm^{-1}), which, in agreement with the theoretical calculations, supports the conclusion that the two electrons simultaneously enter a single Fe_4C unit. Such an aspect, in reality, is somewhat surprising and conceivably reflects the short spectroscopic timescale, in that on the longer electrochemical timescale it is expected that the two electron addition is split in the two carbonyl clusters.

As far as the second reduction of **7** is concerned, Fig.10 shows a fast disappearance of the ν_{CO} bands at 2046 cm^{-1}, 2002 cm^{-1} and 1975 cm^{-1} and a marked increase of the band at 1880 cm^{-1}, whereas the two bands at 1952 and 1926 cm^{-1} remain unaltered.

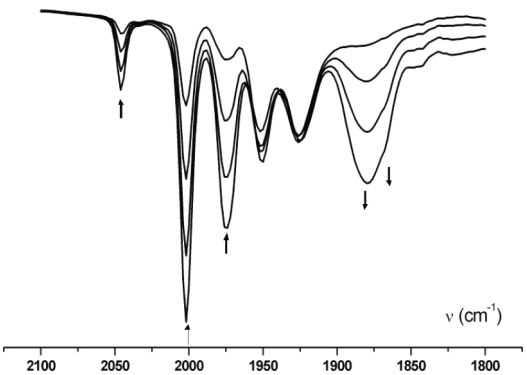

Fig. 10 IR spectroelectrochemical trends in the terminal ν_{CO} region recorded in an OTTLE cell in correspondence of the second reduction of **7**. Stepwise variation (250 μV s^{-1}) of the potential from E_w = – 1.30 V to E_w = – 1.65 V. V *vs.* pseudo-reference Ag electrode. THF solution containing $[NBu_4][PF_6]$ (0.4 mol dm^{-3}) supporting electrolyte.

Even if such a trend is not easily interpreted, it is noteworthy that upon progressive reoxidation, the original IR spectrum is completely restored, confirming the chemical reversibility of the overall reduction pattern.

Considering that there is some voltammetric evidence that, as happens for **4**, the second reduction is centred on the bridged Cu ion, in that also in this case an absorption peak appears in the back-scan due to absorption of Cu(0) species (see asterisked peak in Figure S5 in the Supplementary Material†), it is concluded that, as commented above, the first two-electron reduction implies the simultaneous addition of one electron to each Fe_4C unit, *i.e.* also in this case the two metal carbonyl units are not communicating.

Theoretical calculations

In order to get a better insight into the structural and electronic features of the synthesized clusters, DFT calculations have been carried out on clusters **3–5**, and on clusters $[Fe_4C(CO)_{12}CuPyz]^-$ (**5a**) and $[Fe_4C(CO)_{12}CuCl]^{2-}$ (**5b**),[35] in which the py ligand of cluster **5** is replaced by pyz and Cl^-, respectively. The X-ray structure of the latter cluster differs from those of **3–5** for the geometrical arrangement of the metallic framework, which, in **5b**, is *arachno*-pentagonal bipyramidal with the Fe1–Cu distance equal to about 3.6 Å.[35]

Interestingly, two energy minima on the potential energy surface (PES) are found in the geometry optimization of clusters **3–5**, **5a** and **5b**. The main difference between the two conformational isomers lies in the Fe1–Cu distance. For all clusters the most stable isomer has a square based pyramid framework of metal atoms, with Fe1–Cu distances within 2.77–2.63 Å (relevant geometrical parameters of clusters **3–5**, **5a** and **5b** are reported in the Supplementary Material†). The second isomer of **4**, **5**, **5a**, and **5b** has an *arachno*-pentagonal bipyramid arrangement of the metal atoms, with Fe1–Cu distances longer than 3.5 Å, while the arrangement of the metal atoms in **3** is halfway between square based pyramid and *arachno*-pentagonal bipyramid, with the Fe1–Cu distance equal to 3.13 Å. The calculated Cu1–Fe distance is in good agreement with the experiment for clusters **3**, **5b** (bp geometry) and **4** (sp geometry), while it differs significantly for both isomers in the case of cluster **5**. All other geometrical parameters are very similar in the two isomers, and in fairly good agreement with the X-ray structure (see Supporting Material†).

The energy difference between the two isomers is very small (ΔE = 0.1, 4.0, 3.8, 2.6 and 0.1 kcal mol^{-1} for **3**, **4**, **5**, and **5a** and **5b** respectively) indicating, as suggested above, that the Fe1–Cu interaction is very weak, and that the discrepancy between the calculated and measured value of the Fe1–Cu distance in **5** is indeed due to crystal packing forces.

It is interesting to note that the energy difference between the two isomers is fairly well correlated to the donor/acceptor properties of the ligand coordinated to the Cu atom. In fact, the net charge transferred from the ligand to the metal framework is larger for clusters **3** and **5b**, for which the two isomers are almost isoenergetic (see Table 4). In clusters **4**, **5**, and **5a**, due to the back-bonding donation, a net charge is transferred from the metal framework to the ligand, and the square based pyramid isomer is more stable than the *arachno*-pentagonal bipyramid one. The corresponding charge on the Cu atom clearly depends on the charge transferred from the ligand. The charge is larger for **4**, **5**,

Table 4 NBO charges of clusters **3–5**, **5a** and **5b**. q_L is the charge of the ligand L in the cluster, calculated as a difference between the charge of isolated ligand and the sum of atomic charges of L in the cluster

		q_L	q_{Cu}	q_{Fe1}
3	− 2	− 0.14	+ 0.81	− 0.11
4	− 2	+ 0.08	+ 0.92	− 0.11
5	− 1	+ 0.05	+ 0.91	− 0.11
5a	− 1	+ 0.08	+ 0.92	− 0.11
5b	− 2	− 0.25	+ 0.58	− 0.11

Table 5 Frontier orbital energies and LUMO – HOMO energy gaps $\Delta E_{HO\rightarrow LU}$ (in eV) calculated using the BP86/def-TZVP scheme for the metal clusters **3–5**, **5a**, **5b**, **7** and $[NEt_4]_2$**7**

		ε_{HOMO}	ε_{LUMO}	$\Delta E_{HO\rightarrow LU}$
3	− 2	− 1.19	0.52	*1.71*
4	− 2	− 1.25	− 0.45	*0.80*
5	− 1	− 2.15	− 1.04	*1.11*
5a	− 1	− 2.36	− 1.46	*0.90*
5b	− 2	0.63	2.29	*1.66*
7-mon	− 1	− 2.63	− 1.07	*1.56*
7	− 2	− 1.45	0.02	*1.43*
$[NEt_4]$**7**-mon		− 4.98	− 3.44	*1.54*
$[NEt_4]_2$**7**	0	− 4.97	− 3.51	*1.46*

and **5a** than for **3** and **5b**. The interaction between the Cu atom and the negatively charged Fe1 atom is therefore correlated to the charge of these two centers, explaining the differences in stabilities.

Frontier orbital energies and LUMO–HOMO energy gaps $\Delta E_{HO\rightarrow LU}$ (in eV) of metal cluster **3–5**, **5a**, and **5b** are reported in Table 5. The nature of the ligand coordinated to the $[Fe_4C(CO)_{12}Cu]^-$ core strongly affects the energy gap in these clusters. In fact, the $\Delta E_{HO\rightarrow LU}$ of **4**, **5** and **5a**, where the ligand is pyz or py, is significantly smaller than that of **3**, and **5b** where the ligand is dppe or Cl^-. Interestingly, in the former set of clusters the LUMO is localized on the pyz (or py) ligand, while the HOMO is localized on the $[Fe_4C(CO)_{12}Cu]^-$ core. On the other hand, in **3** and **5b** both HOMO and LUMO are localized on the metallic core. As an example, the frontier orbitals of clusters **3** and **4** are shown in Fig. 11. The comparison of the HOMO (ε_{HOMO}) and LUMO (ε_{LUMO}) energies of these two clusters, which feature the same total charge, clearly indicates that the difference in $\Delta E_{HO\rightarrow LU}$ is due to ε_{LUMO}. In fact, the ε_{HOMO} of **4** and **3** are very similar, confirming the same nature of the HOMO in the two clusters, whereas the ε_{LUMO} of **4** is about 1 eV lower in energy than in **3**, indicating that the localization of the LUMO on the ligand in **4** has the largest impact on the $\Delta E_{HO\rightarrow LU}$.

These results support the electrochemical observations discussed in the previous section.

5a has the same ligand as **4** (pyz), and it features the same total charge as **5** so that the orbital energies of **5** and **5a** can be directly compared.

This comparison shows that the ε_{LUMO} of the latter is about 0.4 eV smaller than that of the former. These values compare well with the trend in the experimental reduction potentials discussed above for **4** and **5** and assigned to the different reduction potential of pyz and py, respectively. It should be noted that $\Delta E_{HO\rightarrow LU}$ of **5a** is slightly smaller than in **5**.

Geometry optimization of the dianion **7** *in vacuo* leads to the dissociation of the cluster into the two $[Fe_4Cu_3C(CO)_{12}(\mu\text{-}pz)_2]^-$ monomeric units. The energy difference between **7**, optimized with

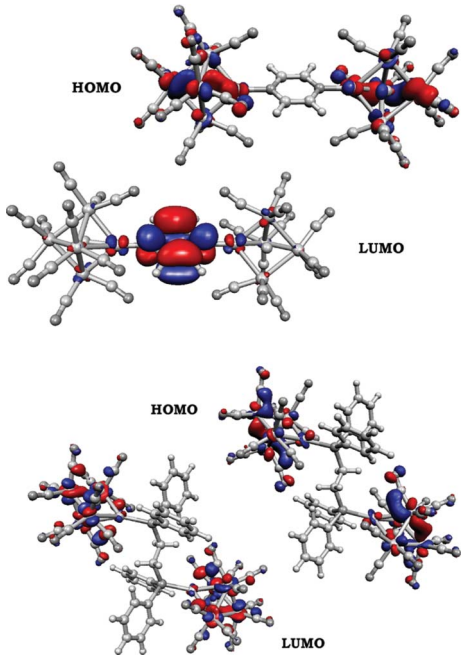

Fig. 11 (a) HOMO and LUMO orbitals of cluster **4**. (b) HOMO and LUMO orbitals of cluster **3**.

the Cu3–Cu6 distance constrained at the X-ray value, and the two isolated monomers (**7**-mon) is equal to about 22 kcal mol^{-1} in favor of the latter, a value that is only slightly smaller (20 kcal mol^{-1}) when the Cu3–Cu6 distance is constrained at 3.20 Å. Clearly, this large ΔE value is not compatible with the presence of the dimeric species in the solid state and (possibly) in solution. The ΔE value can be explained by considering the electrostatic repulsion between the two $[Fe_4Cu_3C(CO)_{12}(\mu\text{-}pz)_2]^{-1}$ units, which largely overwhelms the weak "cuprophilic" interaction between the two Cu atoms. These considerations suggest that counter-ions, and solvent effects could play a relevant role in stabilizing the dimeric species.

In fact, when a geometry optimization is performed on the $[NEt_4]_2$**7** supramolecular system, in which the two NEt_4^+ counter ions are initially placed at their X-ray positions, and the THF solvent is included implicitly using the COSMO approach a completely different result emerges. The cluster $[NEt_4]_2$**7**corresponds to an energy minimum on the potential energy surface with the Cu3–Cu6 distance equal to 2.847 Å. The energy difference between $[NEt_4]_2$**7** and the two neutral $[NEt_4][Fe_4Cu_3C(CO)_{12}(\mu\text{-}pz)_2]$ units ($[NEt_4]$**7**-mon) is equal to about 1 kcal mol^{-1} in favor of the former. Even if the small value of ΔE does not allow us to confirm that the dimeric species is indeed present in solution, we can conclude that the NEt_4^+ ions are essential to keep the two monomeric units close to each other. In this respect we should note that DFT methods generally underestimate intermolecular interactions, and therefore the calculated ΔE value could be considered as a lower limit.

The NEt_4^+ ions in the supramolecular system is a staple for the two monomeric units. These computational results may find further experimental support from the recent DLS measurement, consistent with aggregation of carbonyl clusters in solution in huge particles, possibly constituted by extensive chunks of ionic lattices.[36]

The LUMO and LUMO + 1 of $[NEt_4]_2$**7** (see Fig. 12) are almost degenerate and fully localized over the two different

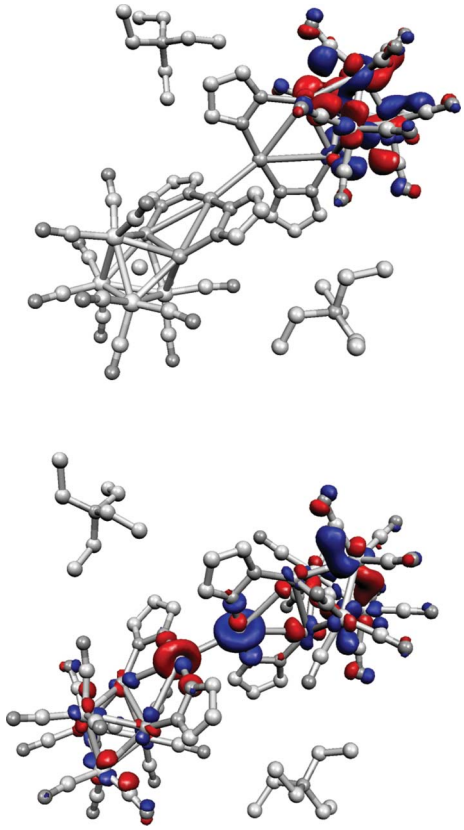

Fig. 12 HOMO and LUMO orbitals of cluster $[NEt_4]_2$**7**.

monomer units. A similar splitting in energy is observed for the other orbitals, and could be ascribed to the interaction with the nonsymmetric NEt_4^+ staples (see the orbital correlation diagram reported in Figure S6 in the Supplementary Material†). In addition, the orbital energies are not significantly affected by the formation of the dimer, since these energies are very similar to those of the separate monomers. Therefore, we can conclude that, in agreement with the above cited spectroelectrochemical findings, there is no electronic communication between the two metal carbonyl units.

Experimental

All the solvents were purified and dried by conventional methods and stored under nitrogen. All the reactions were carried out under an oxygen-free nitrogen atmosphere using the Schlenk-tube technique.[37] $(NEt_4)_2[Fe_5C(CO)_{14}(CuCl)]$,[7] $(NEt_4)_2[Fe_4C(CO)_{12}(CuCl)_2]$,[7] $[Cu(NCMe)_4]PF_6$ [38] and $(NEt_4)_2$-$[Fe_4C(CO)_{12}]$[16] were prepared by literature methods. Infrared spectra in solution were recorded on a Nicolet Avatar 360 FT-IR spectrophotometer, using calcium fluoride cells previously purged with N_2. Elemental analyses were carried out by the staff of Laboratorio di Analisi of the Dipartimento di Chimica Inorganica, Metallorganica e Analitica.

Anhydrous dichloromethane 99.8% was an Aldrich product. Anhydrous 99.9% HPLC-grade tetrahydrofuran (Aldrich) was distilled in the presence of sodium before use. $[NBu_4][PF_6]$ electrochemical grade (Fluka) was used as supporting electrolyte. Cyclic voltammetry was performed in a three electrode cell containing the working electrode surrounded by a platinum-spiral counter electrode, and the reference electrode (Ag/AgCl or SCE) mounted with a Luggin capillary. Platinum, gold or glassy-carbon electrodes were used as working electrodes. For low-temperature measurements, a non-isothermal assembly was set up in which the central part of the cell was enclosed by a thermostatic jacket through which a cooled liquid was circulated.

Controlled potential coulometry was performed in an H-shaped cell with anodic and cathodic compartments separated by a sintered-glass disk. The working macroelectrode was a platinum gauze; a mercury pool was used as the counter electrode. A BAS 100 W electrochemical analyser was used as the polarising unit. All the potential values have been measured with respect to SCE electrode. Under the present experimental conditions, the one-electron oxidation of ferrocene occurs at $E^{\circ\prime}$ = + 0.39 V in dichloromethane, and at $E^{\circ\prime}$ = + 0.54 V in tetrahydrofuran solutions.

IR spectroelectrochemical measurements were carried out using a FT-IR System SPECTRUM BX spectrophotometer. The optically transparent thin-layer cell (OTTLE cell) was constituted by a Pt-minigrid working electrode (32 wires/cm), a Pt minigrid auxiliary electrode, and a Ag wire pseudoreference sandwiched by CaF_2 windows.[39] During controlled potential coulometry, the electrode potential was controlled by an Amel potentiostat 2059 equipped with an Amel function generator 568.

Synthesis of $[Cu(dppe)_2]_2[\{Fe_4C(CO)_{12}Cu\}_2(\mu\text{-dppe})]$ ($[Cu(dppe)_2]_2$3). $[NEt_4]_2[Fe_4C(CO)_{12}(CuCl)_2]$ (0.080 g, 0.070 mmol) and $TlPF_6$ (0.057 g, 0.171 mmol) were dissolved in THF (15 mL). The mixture was stirred at room temperature for 1 h and then filtered; dppe (0.081 g, 0.20 mmol) was added, and the solution stirred for 1 h. The solution was filtered again, and treated with *i*-PrOH (20 mL). The product was precipitated by partial evaporation *in vacuo* and recovered by filtration. The dark solid was dissolved in the minimum amount of THF (*ca.* 5 mL) and layered with *i*-PrOH.

Yield: 62% (0.084 g). Anal. Calc. for $C_{164}H_{136}Cu_4Fe_8O_{26}P_{10}$: C 55.8; H 3.9%. Found. C 55.4; H 4.1%. (Elemental analyses confirm the presence of two solvent molecules). IR ν_{max}(THF)/cm^{-1} 2040(m), 1993(s), 1968(s), 1946(m), 1915(m)

2) Synthesis of $(NEt_4)_2[\{Fe_4C(CO)_{12}Cu\}_2(\mu\text{-pyz})]$ ($(NEt_4)_2$4). A solution of $[NEt_4]_2[Fe_5C(CO)_{14}CuCl]$ (0.14 g, 0.13 mmol) in THF (20 mL) was treated with $AgBF_4$ (0.054 g, 0.27 mmol) and stirred at room temperature for about 2h. Then the white precipitate formed was eliminated by filtration and solid pyrazine (0.023 g, 0.29 mmol) was added in one portion. After stirring overnight, the suspension was filtered and the solution was evaporated to dryness. Crystals suitable for X-Ray analysis were obtained by cautious layering of heptane (10 mL) over the residue dissolved in CH_2Cl_2 (5 mL).

Yield: 69% (0.079 g). Anal. Calc. for $C_{46}H_{44}Cu_2Fe_8N_4O_{24}$: C 34.29; H 2.8%; N 3.5%. Found. 34.4; H 2.9; N 3.4%

IR ν_{max}(THF)/cm^{-1} 2041(mw), 1992(s), 1970(s), 1909(m,br)

^{1}H NMR (d^8-THF)/ppm 8.80(s)

3) Synthesis of $NEt_4[Fe_4C(CO)_{12}Cupy]$ ($NEt_4$5). $[NEt_4]_2[Fe_4C(CO)_{12}]$ (0.23 g; 0.28 mmol), $[Cu(NCMe)_4]PF_6$ (0.10 g; 0.28 mmol) and C_5H_5N (13 μL, 0.28 mmol) were

dissolved in 15 mL of THF, and stirred for 1 h. The solvent was then reduced in vacuum, the clear solution was decanted and layered with heptane. Yield 0.12 g (49%). Anal. Calc. for $C_{26}H_{25}CuFe_4N_2O_{12}$: C 36.98; H 2.98%; N 3.32%. Found. 36.8; H 2.8; N 3.3%. IR ν_{max}(THF)/cm^{-1} 2039(mw), 1989(s), 1967(s), 1909(m,br). ^{1}H NMR (d^8-THF)/ppm 8.79(d, 2), 8.00 (t, 1), 7.60(t, 2)

4) Synthesis of $NEt_4[Fe_4Cu_3C(CO)_{12}(\mu\text{-}S_2CNEt_2)_2]$ ($NEt_4$6). $[NEt_4]_2[Fe_4C(CO)_{12}(CuCl)_2]$ (0.181 g, 0.176 mmol) and $TlPF_6$ (0.137 g, 0.392 mmol) were dissolved in THF (20 mL); after stirring at room temperature for about two hours, the mixture was filtered and to the filtrate $[Cu(NCCH_3)_4]PF_6$ (0.064 g, 0.176 mmol) and $Na(S_2CNEt_2)$ (0.064 g, 0.374 mmol) were added. IR spectroscopy showed the complete conversion into the desired product. The solution was filtered, concentrated under reduced pressure to half volume and layered with heptane. The crystalline product was washed with heptane and dried *in vacuo*. The crystals of $[PPh_4]$**6** used for X-ray analysis were obtained similarly, starting from $[PPh_4]_2$**1**. Yield: 15% (0.032 g). Anal Calc. for $C_{31}H_{40}Cu_3Fe_4N_3O_{12}S_4$: C 31.2; H 3.4; N 3.4%. Found C 31.4; H 3.4; N 3.5%. IR ν_{max}(THF)/cm^{-1} 2042(m), 1997(s), 1972(s), 1951(m), 1931(m)

4) Synthesis of $(NEt_4)_2[\{Fe_4Cu_3C(CO)_{12}(\mu\text{-}pz)_2\}_2]$ ($(NEt_4)_2$7). A mixture of $[NEt_4]_2[(Fe_4C(CO)_{12}(CuCl)_2]$ (0.142 g, 0.183 mmol) and $TlPF_6$ (0.067 g, 0.192 mmol) in THF (10 mL) was stirred at room temperature for about a hour and then filtered. Solid pyrazole (0.025 g, 0.368 mmol) was added to the clear brown filtrate and this solution was stirred in the same conditions described above; the reaction was monitored by IR spectroscopy. When the neutral intermediate $[Fe_4C(CO)_{12}(CupzH)_2]$ was formed, the solution was treated with $[Cu(NCCH_3)_4]PF_6$ (0.072 g, 0.193 mmol) and a slight excess of K_2CO_3. The precipitation of a white powder was completed by dropwise addition of hexane (5 mL), then the suspension was filtered; the solution was evaporated to dryness and crystals of the desired product were obtained from CH_2Cl_2/heptane. Yield: 32% (0.123 g). Anal. Calc. for $C_{55}H_{54}Cl_2Cu_6Fe_8N_{10}O_{24}$: C 30.9; H 2.6; N 6.6%. Found. C 30.5; H 2.4; N 6.8% (Elemental analysis confirms the presence of one solvent molecule). IR ν_{max}(THF)/cm^{-1} 2046(m), 2001(vs), 1974(s), 1930(mw), 1779(w)

^{1}H NMR (d^8-THF)/ppm 7.66(s, 1), 7.44 (s, 1), 6.28(s, 1)

5) X-ray data collections and structure determinations. Crystal data are summarised in Table 6. The diffraction experiments were carried out on a Bruker APEX II CCD area-detector diffractometer at 120, 150, and 296 K. No crystal decay was

Table 6 Crystallographic data

Compound	$[Cu(dppe)_2]_2$**3**·2THF	$[NEt_4]_2$**4**	$[NEt_4]$**5**	$[PPh_4]$**6**	$[NEt_4]_2$**7**·CH_2Cl_2
Formula	$C_{164}H_{136}Cu_4Fe_8O_{26}P_{10}$	$C_{46}H_{44}Cu_2Fe_8N_4O_{24}$	$C_{26}H_{25}CuFe_4N_2O_{12}$	$C_{47}H_{40}Cu_3Fe_4N_2O_{12}PS_4$	$C_{55}H_{54}Cl_2Cu_6Fe_8N_{10}O_{24}$
M	3533.57	1610.73	844.42	1398.09	2138.02
Crystal system	Triclinic	Triclinic	Monoclinic	Monoclinic	Monoclinic
Space group	$P\bar{1}$	$P\bar{1}$	$P2_1/n$	$C2/c$	$P2_1/n$
a/Å	12.2567(7)	10.2603(8)	14.6999(9)	20.3661(10)	13.9712(8)
b/Å	17.5161(10)	11.0569(9)	12.4817(7)	18.7116(9)	26.5870(15)
c/Å	19.6579(11)	14.1750(11)	18.7043(11)	28.4567(14)	20.2166(11)
α (°)	97.503(1)	103.989(1)	90	90	90
β (°)	106.886(2)	104.349(1)	106.510(1)	95.720(1)	94.270(1)
γ (°)	99.215(1)	93.200(1)	90	90	90
U/Å^3	3915.6(4)	1500.2(2)	3290.4(4)	10790.4(9)	7488.7(7)
Z	1	1	4	8	4
$F(000)$	1802	806	1696	5616	4248
D_c/g cm^{-3}	1.498	1.783	1.704	1.721	1.896
Crystal dimensions/mm	0.27 × 0.36 × 0.40	0.05 × 0.23 × 0.41	0.14 × 0.15 × 0.48	0.08 × 0.11 × 0.33	0.31 × 0.35 × 0.38
μ (Mo-Kα)/cm^{-1}	14.17	26.49	24.19	24.47	33.19
Min. and max. *trans*. factors	0.860–1.000	0.721–1.000	0.471–1.000	0.641–1.000	0.839–1.000
T/K	150	296	296	150	120
λ(Mo-Kα)	0.71073	0.71073	0.71073	0.71073	0.71073
Scan mode	ω	ω	ω	ω	ω
Frame width/°	0.33	0.40	0.50	0.30	0.50
Time per frame/s	15	10	35	20	20
No. of frames	3660	1860	1030	3000	2520
Det.-sample distance/cm	6.00	6.00	5.00	6.00	6.00
θ–range	3.00–28.00	3.00–27.00	3.00–28.00	3.00–28.00	3.00–28.00
Reciprocal space explored	full sphere	full sphere	full sphere	full sphere	full sphere
No. of refl. (total; independent)	72908, 19990	19157, 7596	35420, 9504	83984, 14342	159930, 19768
R_{int}	0.0271	0.0307	0.0382	0.0450	0.0299
Final R_2 and R_{2w} indices[a](F^2, all refl.)	0.068, 0.092	0.057, 0.078	0.051, 0.069	0.048, 0.058	0.055, 0.090
Conventional R_1 index ($I > 2\sigma(I)$)	0.040	0.039	0.034	0.030	0.034
Reflections with $I > 2\sigma(I)$	12989	4551	4909	9972	13710
No. of variables	955	379	406	658	949
Goodness of fit[b]	1.046	0.990	0.960	0.975	0.978

[a] $R_2 = [\Sigma(|F_o^2 - kF_c^2|/\Sigma F_o^2]$, $R_{2w} = [\Sigma w(F_o^2 - kF_c^2)^2/\Sigma w(F_o^2)^2]^{1/2}$. [b] $[\Sigma w(F_o^2 - kF_c^2)^2/(N_o - N_v)]^{1/2}$, where $w = 4F_o^2/\sigma(F_o^2)^2$, $\sigma(F_o^2) = [\sigma^2(F_o^2) + (pF_o^2)^2]^{1/2}$, N_o is the number of observations, N_v the number of variables, and p = 0.03 for $[Cu(dppe)_2]_2$**3**·2THF and $[NEt_4]_2$**7**·CH_2Cl_2, and p = 0.02 for $[NEt_4]_2$**4**, $[NEt_4]_2$**5** and $[PPh_4]$**6**.

observed, so that no time-decay correction was needed. The collected frames were processed with the software SAINT,[40] and an empirical absorption correction was applied (SADABS)[41] to the collected reflections. The calculations were performed using the Personal Structure Determination Package[42] and the physical constants tabulated therein.[43] The structures were solved by direct methods (SHELXS)[44] and refined by full-matrix least-squares using all reflections and minimising the function $\Sigma w(F_o^2 - kF_c^2)^2$ (refinement on F^2). In $[NEt_4]_2$**7**·CH_2Cl_2 the solvent molecule is partially disordered, with atoms C37 and Cl1 ordered, and the other chlorine atom split into three peaks, having occupancy factors of 0.50, 0.25, and 0.25, respectively. These last three chlorine atoms were refined isotropically, and the two hydrogen atoms of the molecule were ignored. All the other non-hydrogen atoms were refined with anisotropic thermal factors. In $[Cu(dppe)_2]_2$**3**·2THF, in which the anion lies on a crystallographic inversion center, hydrogen atoms H1 and H2, bonded to the ethylic carbon atom C13, were detected in the final Fourier maps and not refined. Similarly, in $[NEt_4]_2$**4**, hydrogen atoms H1 and H2, bonded to the pyrazinic carbon atoms C13 and C14, respectively, were detected in the final Fourier maps and not refined. All the other, non-mentioned hydrogen atoms were placed in their ideal positions (C–H = 0.97 Å), with the thermal parameter U being 1.10 times that of the carbon atom to which they are attached, and not refined. In the final Fourier maps the maximum residuals were 1.82(25) eÅ^{-3} at 1.30 Å from Fe(1) (for $[Cu(dppe)_2]_2$**3**·2THF) 0.90(29) eÅ^{-3} at 1.58 Å from N(2) (for $[NEt_4]_2$**4**) 0.58(27) eÅ^{-3} at 1.63 Å from C(5) (for $[NEt_4]$**5**), 0.77(29) eÅ^{-3} at 0.09 Å from Cu(1) (for $[PPh_4]$**6**) and 2.18(36) eÅ^{-3} at 1.60 Å from N(10) (for $[NEt_4]_2$**7**·CH_2Cl_2). Minimum peaks (holes), in the same order, were – 0.98(25), – 0.70(29), – 0.50(27), – 0.84(29), and – 1.52(36) e·Å^{-3}.

6) Computational methods. DFT calculations have been carried out using the pure functional BP86[45,46] and an all-electron valence triple-ζ basis set with polarization on all atoms (TZVP).[47] Calculations have been carried out with the TURBOMOLE 5.9 suite[48] applying the resolution-of-the-identity technique.[49,50]

Stationary points of the energy hypersurface have been located by means of energy gradient techniques.

Geometry optimizations and energy calculations of clusters $[NEt_4]_2$**7**-mon and $[NEt_4]_2$**7** have been carried out for their THF solutions (ε = 7.426), modelled by using the *Conductor Screening Model* (COSMO)[51] approach implemented in TURBOMOLE 5.9. All other calculations have been performed *in vacuo*. Charge population analyses have been computed according to the Natural Atomic Orbital scheme.[52]

Conclusions

The copper sites of $[Fe_4C(CO)_{12}Cu_x]$ clusters (x = 1–3) can be used to connect them with bridging ligands, constructing oligomeric or polymeric structures. The ammonium salts of **4** and **7** are well soluble and therefore suitable for electrochemical experiments, to ascertain the eventual electronic communication between the metallic units. Despite the presence of definite M–L bonds in **4**, and a weaker cuprophilic interaction in **7**, communication between the two clusters is absent in both. Even if multi-copper assemblies frequently display fluorescence properties,[53] preliminary experiments seem to exclude interesting features for **7**. The self-assembled structures of the $[Fe_4Cu_3C(CO)_{12}(\mu\text{-}L)_2]^-$ anions suggest that staple arrays are not limited to thiolate-covered gold particles, but can be formed by other ligands and other metals, including copper. In agreement, staples were also found in thiolate covered silver clusters.[54] Some heterometallic Fe–Cu–Hg arrays have already been reported for carbonyl species.[55] Cyclic Fe–Hg–Pd[56] structures are formed even without elements of group 11. Therefore, we are testing the ability of the $[Fe_4Cu_3(CO)_{12}(\mu\text{-}L)_2]^-$ anions to clamp other metallic ions in linear geometry (such as Hg^{2+} or Ag^+) and we are using cations with higher coordination numbers (such as Ni^{2+}, Pd^{2+}, Cu^{2+}, or Zn^{2+}) to achieve our original goal, the formation of coordination polymers.

Acknowledgements

This work was funded by PRIN 2007 (RDP, MM), PRIN 2008 (PZ) and University of Milano Bicocca (AS and MB)

References

1 G. Peli, M. Daghetta, P. Macchi, A. Sironi and L. Garlaschelli, *Dalton Trans.*, 2010, 1188.
2 I. O. Koshevoy, M. Haukka, T. A. Pakkanen, S. P. Tunik and P. Vainiotalo, *Organometallics*, 2010, **34**, 3516.
3 R. Della Pergola, A. Sironi, C. Manassero and M. Manassero, *Eur. J. Inorg. Chem.*, 2009, 4618.
4 C. Femoni, M. C. Iapalucci, F. Kaswalder, G. Longoni and S. Zacchini, *Coord. Chem. Rev.*, 2006, **250**, 1580.
5 M. Shieh, C.-H. Ho, W.-S. Sheu, B.-G. Chen, Y.-Y. Chu, C.-Y. Miu, H.-L. Liu and C.-C. Shen, *J. Am. Chem. Soc.*, 2008, **130**, 14114.
6 M. Shieh, M.-H. Hsu, W.-S. Sheu, L.-F. Jang, S.-F. Lin, Y.-Y. Chu, C.-H. Miu, Y.-W. Lai, H.-L. Liu and J. L. Her, *Chem.–Eur. J.*, 2007, **13**, 6605.
7 R. Della Pergola, A. Sironi, L. Garlaschelli, D. Strumolo, C. Manassero, M. Manassero, S. Fedi, P. Zanello, F. Kaswalder and S. Zacchini, *Inorg. Chim. Acta*, 2010, **363**, 586–594.
8 C. Femoni, R. Della Pergola, M. C. Iapalucci, F. Kaswalder, M. Riccò and S. Zacchini, *Dalton Trans.*, 2009, 1509.
9 P. D. Jadzinsky, G. Calero, C. J. Ackerson, D. A. Bushnell and R. D. Kornberg, *Science*, 2007, **318**, 430.
10 P. Leoni, M. Pasquali and C. A. Ghilardi, *J. Chem. Soc., Chem. Commun.*, 1983, 240.
11 F. M. Woodward, P. J. Gibson, G. B. Jameson, C. P. Landee, M. M. Turnbull and R. D. Willett, *Inorg. Chem.*, 2007, **46**, 4256.
12 (*a*) G. La Monica and G. A. Ardizzoia, *Prog. Inorg. Chem.*, 1997, **46**, 151; (*b*) M. A. Halcrow, *Dalton Trans.*, **2009**, 2059–2073.
13 M Bonamico, G. Dessy, A. Mugnoli, A. Vaciago and L. Zambonelli, *Acta Crystallogr.*, 1965, **19**, 886.
14 S. J. Berners-Price, R. K. Johnson, C. K. Mirabelli, L. F. Faucette, F. L. McCabe and P. J. Sadler, *Inorg. Chem.*, 1987, **26**, 3383.
15 A. Marker and M. J. Gunter, *J. Magn. Reson.*, 1982, **47**, 118.
16 E. W. Hill and J. S. Bradley, *Inorg. Synth.*, 1990, **27**, 182–187.
17 M. Y. Darensbourg, *Prog. Inorg. Chem.*, 1985, **33**, 221.
18 G. Doyle, K. A. Eriksen and D. Van Engen, *J. Am. Chem. Soc.*, 1985, **107**, 7914.
19 A. Gourdon and Y. Jeannin, *J. Organomet. Chem.*, 1985, **290**, 199.
20 (*a*) P. F. Jackson, B. F. G. Johnson, J. Lewis and J. N. Nicholls, *J. Chem. Soc., Chem. Commun.*, 1980, 564; (*b*) B. F. G. Johnson, J. Lewis, J. N. Nicholls, J. Puga, P. R. Raithby, M. J. Rosales, M. McPartlin and W. Clegg, *J. Chem. Soc., Dalton Trans.*, 1983, 277.
21 V. Yempally, L. Zhu and B. Captain, *J. Cluster Sci.*, 2009, **20**, 695–705.
22 P. Maksymovych, D. C. Sorescu and J. T. Yates, *Phys. Rev. Lett.*, 2006, **97**, 146103.
23 H. Qian, W. T. Eckenhoff, Y. Zhu, T. Pintauer and R. Jin, *J. Am. Chem. Soc.*, 2010, **132**, 8280.
24 M. W. Heaven, A. Dass, P. S. White, K. M. Holt and R. W. Murray, *J. Am. Chem. Soc.*, 2008, **130**, 3754.
25 D. Jiang, M. L. Tiago, W. Luo and S. Dai, *J. Am. Chem. Soc.*, 2008, **130**, 2777.

26 Z. Tang, B. Xu, B. Wu, M. W. Germann and G. Wang, *J. Am. Chem. Soc.*, 2010, **132**, 3367.
27 H. L. Hermann, G. Boche and P. Schwerdtfeger, *Chem.–Eur. J.*, 2001, **7**, 5333.
28 J. Ribas Gispert, *Coordination Chemistry*, Wiley-VCH, Weinheim, 2008 pp. 134.
29 M. Tachikawa and E. L. Muetterties, *J. Am. Chem. Soc.*, 1980, **102**, 4541.
30 P. Zanello, *Inorganic Electrochemistry. Theory, Practice and 31. Application*, Royal Society of Chemistry, United Kingdom, 2003.
31 K. B. Wiberg and T. P. Lewis, *J. Am. Chem. Soc.*, 1970, **92**, 7154.
32 V. W.-W. Yam and K. K.-W. Lo, *J. Chem. Soc., Dalton Trans.*, 1995, 499.
33 P. L. Bogdan, C. Woodcock and D. F. Shriver, *Organometallics*, 1987, **6**, 1377.
34 S. Fedi, P. Zanello, F. Laschi, A. Ceriotti and S. El Afefey, *J. Solid State Electrochem.*, 2009, **13**, 1497.
35 R. Della Pergola, A. Sironi, C. Manassero and M. Manassero, *Organometallics*, 2010, **29**, 5885.
36 (*a*) C. Femoni, M. C. Iapalucci, G. Longoni, T. Lovato, S. Stagni and S. Zacchini, *Inorg. Chem.*, 2010, **49**, 5992; (*b*) A. Bernardi, C. Femoni, M. C. Iapalucci, G. Longoni and S. Zacchini, *Dalton Trans.*, 2009, 4245.
37 D. F. Shriver, M. A. Drezdzon, *The Manipulation of air-sensitive compounds*, Wiley, New York, 2nd ed. 1986.
38 G. J. Kubas, *Inorg. Synth.*, 1990, **28**, 68–70.
39 M. Krejčik, M. Daněk and F. Hartl, *J. Electroanal. Chem.*, 1991, **317**, 179.
40 *SAINT* Reference manual, Siemens Energy and Automation, Madison, WI, 1994–1996.
41 G. M. Sheldrick, *SADABS*, Empirical Absorption Correction Program, University of Gottingen, Germany, 1997.
42 B. A. Frenz, *Comput. Phys.*, 1988, **2**, 42.
43 *Crystallographic Computing 5*, Oxford University Press, Oxford, U.K., 1991, Chapter 11, p. 126.
44 G. M. Sheldrick,(1985) *SHELXS 86*. Program for the solution of crystal structures. University of Gottingen, Germany.
45 J. P. Perdew, *Phys. Rev. B*, 1986, **33**, 8822–8824.
46 A. D. Becke, *Phys. Rev. A: At., Mol., Opt. Phys.*, 1988, **38**, 3098–3100.
47 A. Schafer, C. Huber and R. Ahlrichs, *J. Chem. Phys.*, 1994, **100**, 5829–5835.
48 R. Ahlrichs, M. Bar, M. Haser, H. Horn and C. Kolmel, *Chem. Phys. Lett.*, 1989, **162**, 165–169.
49 K. Eichkorn, O. Treutler, H. Ohm, M. Haser and R. Ahlrichs, *Chem. Phys. Lett.*, 1995, **240**, 283–289.
50 K. Eichkorn, F. Weigend, O. Treutler and R. Ahlrichs, *Theor. Chem. Acc.*, 1997, **97**, 119–124.
51 A. Klamt, *J. Phys. Chem.*, 1995, **99**, 2224–2235.
52 A. E. Reed, L. A. Curtiss and F. Weinhold, *Chem. Rev.*, 1988, **88**, 899–926.
53 V. W.-W. Yam and K K.-W. Lo, *Chem. Soc. Rev.*, 1999, **28**, 323.
54 X. Liu, H. Yang, N. Zheng and L. Zheng, *Eur. J. Inorg. Chem.*, 2010, 2084.
55 M. Bénard, U. Bodensiek, P. Braunstein, M. Knorr, M. Strampfer and C. Strohmann, *Angew. Chem., Int. Ed. Engl.*, 1997, **36**, 2758.
56 W. Schuh, P. Braunstein, M. Bénard, M.-M. Rohmer and R. Welter, *Angew. Chem., Int. Ed.*, 2003, **42**, 2161.